ChemComm

Accepted Manuscript

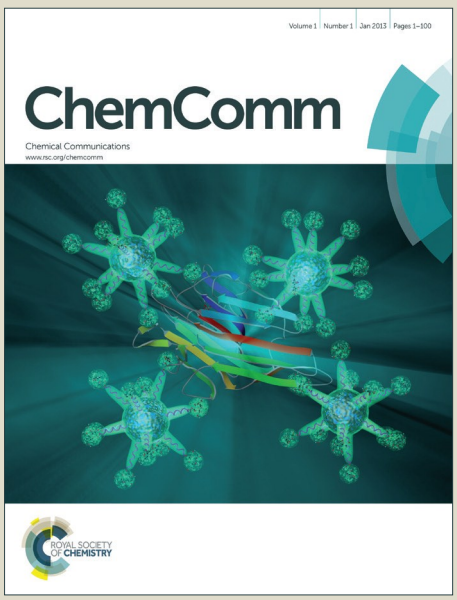

ROYAL SOCIETY OF CHEMISTRY

www.rsc.org/chemcomm

Chem Comm

COMMUNICATION

Biomorph Growth in Single-Phase Systems: Expanding the Structure Spectrum and pH Range

Received 00th January 20xx,
Accepted 00th January 20xx

DOI: 10.1039/x0xx00000x

www.rsc.org/

Elias Nakouzi, Pamela Knoll, and Oliver Steinbock*

Biomorphs are life-like microstructures of selfassembled barium carbonate nanorods and silica. In a departure from established approaches, we produce biomorphs in CO_2- and gradient-free solutions. Our study reveals novel structural motifs for solution-grown biomorphs, reduces pH transients, and expands the upper pH limit for biomorph formation to over 12 where silica is essentially soluble.

A fundamental challenge for materials chemistry is to utilize the self-assembly of nanostructures for the production of mesoscopic objects that in their structural complexity exceed the limited symmetry repertoire of crystallography.[1,2] Advances towards this goal could ultimately lead to a new engineering paradigm under which complex materials and devices are not assembled sequentially but grown in a parallel fashion.[3–5] To date examples for such processes are essentially limited to biomineralized structures including nacre, bone, and tooth enamel.[6,7] However, similar processes can exist in inorganic chemistry.[8–10] In this context, hierarchically ordered, polycrystalline aggregates called biomorphs, are the prime example.[11–13] These microstructures have smoothly curved morphologies such as cardioidal sheets, stemmed cones, and helices.[14–18] At the nanoscale, they consist of densely packed crystalline barium carbonate nanorods and amorphous silica. The nanorod assemblies have a strict long-range order that is tightly coupled to the thousand times larger shapes of the microstructures.

Biomorphs are produced from aqueous solutions of barium and silicate ions by diffusive influx of carbon dioxide from the air.[15] The resulting crystallization of witherite, a form of barium carbonate, is affected by silica precipitation causing the growth of high-aspect ratio nanorods with a width of around 40 nm.[19] The rates of the two precipitation processes are pH-dependent and suggest a possible oscillatory mechanism in which witherite formation lowers the pH to prompt silica precipitation which in turn raises the pH to reignite the witherite growth. Accordingly, biomorph growth has been observed mostly within a pH window of 10 to 11 because silica becomes increasingly soluble at higher values. Here, we report an experimental approach that expands the biomorph-forming reaction conditions and in doing so conflicts with the aforementioned mechanism. In addition, we observe several, novel biomorph structures that extend biomorphs to lengthscales of millimeters.

In contrast to earlier studies, our experiments exclude CO_2 and induce witherite growth strictly from dissolved sodium carbonate. This modification creates an initially homogeneous reaction medium that is not subject to concentration gradients caused by the influx of atmospheric CO_2. Nonetheless, these conceptually simpler reaction conditions induce the formation of a multitude of biomorphs. Figure 1 shows a collage of the most striking shapes encountered in our experiments. The examples in Figs. 1a-c are a substrate-bound cardioidal sheet, a double helix, and a worm-like single helix, respectively. These structures represent the three classical motifs that are well known from earlier gas-diffusion studies but also readily found in our experiments. The two image rows below show novel structures that are best described as freely curving sheets (d,e), hollow urns (f), and funnels (g).

The latter sheets are remarkable as they are not bound to the substrate demonstrating that growth of thin biomorph foils does require a planar template. Furthermore, they are folded into C- and S-shaped structures. Their edge features a thicker zone of crystallites (black arrows) that typically cause a local cessation of the sheet expansion. The micro-urn (f) has a diameter of about 40 µm that varies smoothly along the symmetry axis of the structure. Its cross-section is remarkably circular which suggests that surface tension or elastic forces might be active during the assembly. It is also interesting to speculate whether the solution in the interior of the urn differs from the exterior medium as concentration gradients could cause the smooth diameter variation of the urn. The funnel (g) is the largest structure and features two small urns at its rim (black arrows). The funnel's outer surface is strictly concave and its diameter, which increases rapidly in the upward image direction, diverges to yield a near planar sheet. This

[a] *Florida State University, Department of Chemistry and Biochemistry, Tallahassee, FL 32306-4390.*
* Corresponding author. Email: steinbck@chem.fsu.edu
Electronic Supplementary Information (ESI) available: Additional optical and electron micrographs of curved sheets and concave funnels. ATR-IR spectrum of the biomorphs formed at pH > 12. Details of the image correlation analysis. Movie showing the growth of the curved sheets. See DOI: 10.1039/x0xx00000x

structure is markedly different from the smaller, linear cones in a recent study by the Aizenberg group.[13] We note that the curved sheets and concave funnel structures have been observed before in gel-based systems,[11] but not for solution-grown biomorphs.

We also observe a variety of erratic biomorph shapes including curved rods and striped structures reminiscent of marine shells (Fig. 1h). For other reactant concentrations, non-biomorphic aggregates such as needles and spherulites are observed (Figure 1i). These morphologies are characteristic of barium carbonate microcrystals and are known from other systems.[20,21] The crystals can also grow into micro-prisms with crystallographic morphologies (Fig. 1j). Finally, the dense aggregates in Fig. 1k are similar to the precursor globules that eventually evolve into biomorphs (Fig. 1a, black arrow). However, the chemical conditions are not favorable for biomorph assembly and the growth ceases at the globule stage.

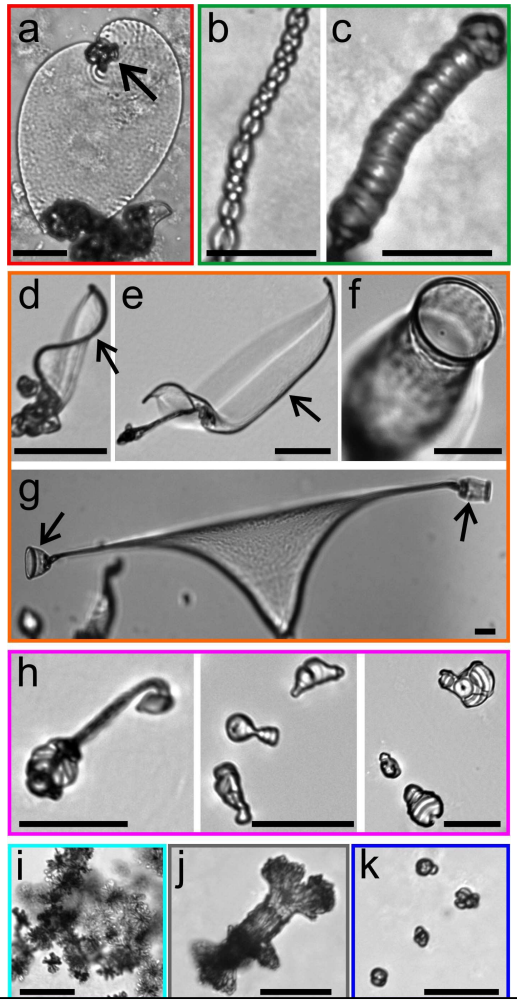

Fig. 1 Optical micrographs of structures obtained in the closed, single-phase system. Classic biomorphs: (a) cardioidal leaves, (b) double helices, (c) single helices. Novel biomorphs: (d, e) curved sheets, (f) convex urns, (g) concave funnels, (h) other structures. Non-biomorphic patterns: (i) witherite needles, (j) prismatic crystals, (k) globular aggregates. Scale bars: 40 µm.

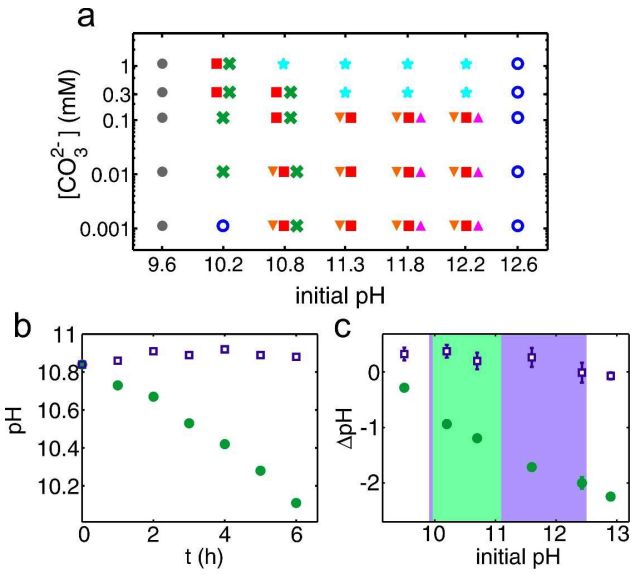

Fig. 2 (a) Phase diagram of morphologies obtained with $[Ba^{2+}]$ = 5 mM, $[SiO_3^{2-}]$ = 8.4 mM: planar sheets (red squares), single and double helices (green crosses), curved sheets and thin-walled assemblies (orange, downwards triangles), other biomorphs (magenta, upwards triangles), witherite needles (cyan pentagrams), prisms (grey, filled circles), and globules (blue, open circles). (b) The change in solution pH in the single-phase (open squares) and two-phase system (filled circles). (c) ΔpH over 18 hours for the single-phase system (open squares) and the two-phase system (filled circles). The purple and green shaded areas indicate the biomorph-yielding pH conditions in the single- and two-phase systems, respectively.

Figure 2a is a phase diagram (or "morphodrome") of the various microstructures in terms of initial pH and carbonate concentration. Note that the latter quantity corresponds to the total amount of carbonate species in the system and is not calculated from the equilibrium speciation at different pH values. Several important trends are discernible from the phase diagram. Firstly, the relatively higher carbonate concentrations tend to produce needles and spherulites (cyan, pentagram markers), which is consistent with literature reports.[21] At the highest probed pH values, the globular aggregates do not lead to the formation of biomorphs (blue, open circles). This result is expected since silica–an essential component in biomorph assembly–is effectively soluble at pH > 12.6. On the acidic side of the pH spectrum, the silica species tend to rapidly coagulate into gels. As a result, the subtle silica-carbonate co-precipitation is disrupted and we obtain faceted witherite prisms (grey, filled circles).

The biomorph-yielding reaction conditions in the phase diagram show the following general trends. Lower carbonate concentrations are required for the synthesis of biomorphs at higher pH values. This observation is related to the decreasing solubility of barium carbonate at increased pH. Among the various biomorph shapes, the planar sheets (red squares) are the most ubiquitous and observed over a wide pH range of 10 to 12.4. By comparison, the

single and double helices (green crosses) form at pH < 11 and typically co-exist in the same crystallization solutions. Finally, the curved sheets, urns, and funnels (orange, downwards triangles) tend to assemble in highly alkaline solutions of pH > 10.8.

Our results so far raise the question why the new single-phase conditions produce structures that are not known from gas-diffusion experiments. The answer to this question is tightly related to temporal changes in solution pH. Figure 2b compares the pH evolution in a closed, carbonate-controlled (open squares) and an open, CO_2-mediated reaction system (filled circles). In this example, the initial pH of both systems was adjusted to 10.8 and also all other reaction conditions were identical. Over a period of 6 h, the data show a nearly linear decrease to 10.1 for the open system, whereas the closed system essentially maintains a constant pH. This difference is clearly caused by a continuous CO_2-induced acidification. Figure 2c summarizes the magnitude of the pH change over 18 h as a function of the initial pH. Again we find that the pH under single-phase conditions is stable, while the gas-diffusion method induces changes of up to two units.

Due to these transient conditions, the formation of biomorphs in the gas-diffusion system is limited to a narrower range of initial conditions (Fig. 2c, green shaded area). In contrast, the isolated, single-phase system excludes acidification and is hence more conducive to biomorph synthesis over a wider pH range (Fig. 2c, purple shaded area). Moreover, the chemical conditions in this system remain stable over several weeks, allowing the assembly of unusually large biomorph sheets, funnels, and helices that extend to lengthscales of several millimeters (Fig. S1). These structures are more than ten times larger than the conventional biomorphs in the two-phase system. Among these macrobiomorphs are novel structures that are reminiscent of wavy curtains (Fig. 3a,b). Their smooth, often Ω-shaped sheet undulations have wavelengths of about 50-100 µm exceeding the total size of conventional biomorphs grown from solutions. Moreover, the surface areas of these convoluted curtains are comparable to and even extend beyond the size of biomorphs grown in gel media, which are typically more expansive.

Biomorph formation at a high pH of more than 12 is extremely surprising. As we mentioned earlier, the solubility of silica comfortably exceeds 0.1 M at these conditions and our results thus cloud earlier mechanistic suggestions that are based on simple or oscillatory co-precipitation. This topic is further complicated by the lack of information on the location of silica in the biomorphs. While compositional analyses yield mole percentages of up to 40% silica, X-ray diffraction (XRD) measurements show predominantly witherite patterns.[15] Moreover, at pH > 12 the formation of barium carbonate competes with barium hydroxide. We hence perform additional experiments to analyze the composition and nanostructure of the high-pH biomorphs. Figure 3c shows the powder-XRD pattern of biomorphs formed at pH 12.2, which include curved sheets, urns, and funnels. The pattern shows the characteristic peaks of barium carbonate (witherite) crystals and hence supports our identification of the structures as biomorphs.

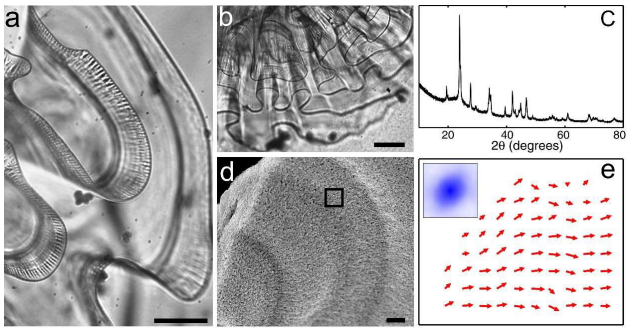

Fig. 3 (a,b) Complex, wavy curtains in the single-phase system. (c) PXRD pattern shows the characteristic witherite peaks. (d) FE-SEM image of micro- and nanoscale features on the curved sheet surface. (e) Vector field of nanorod alignment calculated using image correlation analysis. The inset shows the anisotropic correlation map of the black sub-frame in (d). Scale bars (a,b) 100 µm, (c) 1 µm.

Additional evidence is presented in the scanning electron micrograph in Fig. 3d. This example is a free-growing sheet similar to those in Fig. 1d,e. Qualitative inspection of the image reveals ordered assemblies of elongated nanocrystals that are characteristic of biomorphs. To obtain a more detailed description of the local nanorod alignment, we compute the two-dimensional autocorrelation function for each image pixel. Local averaging produces anisotropic correlation maps (inset of Fig. 3e) in which the long axis indicates the average nanorod orientation. Figure 3d collates these orientations as a vector field that corresponds to the SEM image in Fig. 3d (arrow heads point in growth direction). The result reveals the high degree of radial alignment expected for biomorph sheets.

In addition, we measure the sheet thickness as 1–2 µm, which is similar to the earlier reported average thickness of surface-bound sheets.[22] Interestingly, the biomorph surface also shows topographic modulations that in the SEM image take the form of oscillatory bands. Similar features have recently been observed in planar sheets and are ascribed to the periodic out-of-plane tilting of the carbonate nanorods.[22] These features are recovered as small directional variations in Fig. 3d. The wavelength of the curved sheet oscillations measures approximately 6 µm and is therefore comparable to the value reported for planar sheets.

In conclusion, our study establishes that biomorphs can grow in the absence of CO_2 and transport-related, macroscopic gradients. The substitution of gaseous CO_2 with dissolved carbonate yields superior reaction conditions that offer stable pH conditions and greatly increased reaction times. Indeed, under our conditions biomorph growth can continue for several weeks. Accordingly, we observe larger structures that should be of great value for future quantitative measurements of the biomorphs' mesoscopic characteristics such as the wavelength and period of helices as well as their dispersion relation. Our new approach also raises the upper pH limit to a highly interesting range in which the silica chemistry is markedly different. Future studies should evaluate the location and distribution of silica within the biomorph. Our results already

indicate that the local pH near the expanding biomorph surface must be lower than the bulk solution pH. Accordingly, more systematic measurements are needed to probe the chemical environment near the growing interface.[23] Detailed understanding of these factors appears essential for the development of a growth mechanism that could yield clues for the application of biomorphic nano-to-micro coupling to other materials.

This work was supported by the National Science Foundation under Grant No. 1005861. The High Performance Materials Institute at Florida State University provided access to the FE-SEM facility. EN acknowledges the Mineralogical Society of America (MSA) and the International Centre for Diffraction Data (ICDD).

Notes and references

1 H. Cölfen and M. Antonietti, *Mesocrystals and Nonclassical Crystallization*, John Wiley & Sons, Ltd., Chichester, UK, 2008.
2 (*a*) S. Mann, *Nat. Mater.*, 2009, **8**, 781–792. (*b*) G. M. Whitesides, *Angew. Chem. Int. Ed.,* 2015, **54**, 3196–3209.
3 B. A. Grzybowski, *Chemistry in motion: reaction-diffusion systems for micro- and nanotechnology*, John Wiley and Sons, Chichester, UK, 2009.
4 R. Makki, M. Al-Humiari, S. Dutta, and O. Steinbock, *Angew. Chem. Int. Ed.*, 2009, **48**, 8752–8756.
5 (*a*) F. Haudin, J. H. E. Cartwright, F. Brau, and A. De Wit, *Proc. Natl. Acad. Sci. USA*, 2014, **111**, 17363–17367. (*b*) O. Steinbock, *Proc. Natl. Acad. Sci. USA,* 2014, **111**, 17346-17347.
6 (*a*) P. M. Dove, J. J. De Yoreo, and S. Weiner, *Biomineralization*, Mineralogical Society of America, Washington D. C., 2003, vol. 54. (*b*) J. J. De Yoreo, P. U. P. A. Gilbert, N. A. J. M. Sommerdijk, R. L. Penn, S. Whitelam, D. Joester, H. Zhang, J. D. Rimer, A. Navrotsky, J. F. Banfield, A. F. Wallace, F. M. Michel, F. C. Meldrum, H. Colfen, and P. M. Dove, *Science*, 2015, **349**, aaa6760/1-9.
7 J. Aizenberg, *MRS Bull.*, 2010, **35**, 323–330.
8 (*a*) L. M. Barge, S. S. S. Cardoso, J. H. E. Cartwright, G. J. T. Cooper, L. Cronin, A. De Wit, I. J. Doloboff, B. Escribano, R. E. Goldstein, F. Haudin, D. E. H. Jones, A. L. Mackay, J. Maselko, J. J. Pagano, J. Pantaleone, M. J. Russell, C. I. Sainz-Díaz, O. Steinbock, D. A. Stone, Y. Tanimoto, and N. L. Thomas, *Chem. Rev.*, 2015, **115**, 8652–8703. (*b*) B. C. Batista and O. Steinbock, Chem. Comm., 2015, **51**, 12962-12965.
9 (*a*) L. B. Gower and D. J. Odom, *J. Cryst. Growth*, 2000, **210**, 719–734. (*b*) L. B. Gower, *Chem. Rev.*, 2008, **108**, 4551–4627.
10 (*a*) E. Asenath-Smith, H. Li, E. C. Keene, Z. W. Seh, and L. A. Estroff, *Adv. Funct. Mater.*, 2012, **22**, 2891–2914. (*b*) E. Asenath-Smith, R. Hovden, L. F. Kourkoutis, and L. A. Estroff, *J. Am. Chem. Soc.*, 2015, **137**, 5184–5192.
11 (a) J. M. García-Ruiz, S. T. Hyde, A. M. Carnerup, A. G. Christy, M. J. Van Kranendonk, and N. J. Welhalm, *Science*, 2003, **202**, 1194–1197. (b) J. M. García-Ruiz, A. M. Carnerup, A. G. Christy, N. J. Welham, and S. T. Hyde, *Astrobiology, 2002,* **2**, 353-369.
12 J. M. García-Ruiz, E. Melero-García, and S. T. Hyde, *Science*, 2009, **323**, 362–365.
13 W. L. Noorduin, A. Grinthal, L. Mahadevan, and J. Aizenberg, *Science*, 2013, **340**, 832–837.
14 E. Bittarello, F. R. Massaro, and D. Aquilano, *J. Cryst. Growth*, 2010, **312**, 402–412.
15 (a) M. Kellermeier, H. Cölfen, and J. M. García-Ruiz, *Eur. J. Inorg. Chem.*, 2012, **2012**, 5123–5144. (b) J. M. García-Ruiz, *SEPM Special Publication*, 67, **2000**, 75–89. (c) J. M. García-Ruiz, *Geology*, 26, **1998**, 843–846.
16 J. Eiblmeier, M. Kellermeier, M. Deng, L. Kienle, J. M. García-Ruiz, and W. Kunz, *Chem. Mater.*, 2013, **25**, 1842−1851.
17 J. Eiblmeier, S. Dankesreiter, A. Pfitzner, G. Schmalz, W. Kunz, and M. Kellermeier, *Cryst. Growth Des.*, 2014, **14**, 6177–6188.
18 G. Wang, X. Zhao, M. Möller, and S. E. Moya, *ACS Appl. Mater. Interfaces*, 2015, in press.
19 J. Eiblmeier, U. Schürmann, L. Kienle, D. Gebauer, W. Kunz, and M. Kellermeier, *Nanoscale*, 2014, **6**, 14939–14949.
20 P.-C. Chen, G. Y. Cheng, M. H. Kou, P. Y. Shia, and P. O. Chung, *J. Cryst. Growth*, 2001, **226**, 458–472.
21 S.-H. Yu, H. Cölfen, A.-W. Xu, and W. Dong, *Cryst. Growth Des.*, 2004, **4**, 33–37.
22 E. Nakouzi, Y. E. Ghoussoub, P. Knoll, and O. Steinbock, *J. Phys. Chem. C*, 2015, **119**, 15749–15754.
23 J. Opel, M. Hecht, K. Rurack, J. Eiblmeier, W. Kunz, H. Cölfen, and M. Kellermeier, *Nanoscale*, 2015, **7**, 17434–17440.